Analysis of the Retrogradation of Low Starch Concentration Gels Using Differential Scanning Calorimetry, Rheology, and Nuclear Magnetic Resonance Spectroscopy

Kenneth S. Lewen,[†] Teri Paeschke,[‡] Joshua Reid,[§] Paul Molitor,[||] and Shelly J. Schmidt*,[‡]

General Mills, 9000 Plymouth Avenue North, Minneapolis, Minnesota, Department of Food Science and Human Nutrition, University of Illinois, 905 South Goodwin Avenue, 367 Bevier Hall, Urbana, Illinois 61801, Whistler Center for Carbohydrate Research, Purdue University, 1160 Food Science Building, West Lafayette, Indiana 47907, and VOICE NMR Lab, University of Illinois, 600 South Mathews, 31-1 Noyes Lab, Urbana, Illinois 61801

The retrogradation of 5, 10, 15, and 25% corn starch gels was measured using differential scanning calorimetry (DSC), rheology, and an array of NMR spectroscopy techniques. During the initial (<24 h) stage of retrogradation, an increase in G' corresponding to an increase in the number of solid protons participating in cross-relaxation (M_0^B) was observed for all four concentrations studied. During the latter (>24 h) stage of retrogradation, amylopectin recrystallization becomes the dominant process as measured by an increase in ΔH_r for the 25% starch gel, which corresponded to a further increase in M_0^B. A decrease in the molecular mobility of the liquid component was observed by decreases in ^{17}O T_2, ^1H D_0, and T_{2A}. The value for T_{2B} (the solid transverse relaxation time) did not change with concentration or time indicating that the mobility of the solid component does not change over time despite the conversion of the highly mobile starch fraction to the less mobile solid state during retrogradation.

KEYWORDS: Corn starch; nuclear magnetic resonance spectroscopy; cross-relaxation; differential scanning calorimetry; rheology

INTRODUCTION

Food materials that are semisolids, suspensions, slurries, or emulsions owe most of their functional properties to the dynamic network of bonds and molecular assemblies that make up their structure. Starch, a major component of numerous food products, is used to control the viscosity and texture of these types of food materials. Starch functionality depends on the molecular structure of the amylose and amylopectin components and their interaction with their environment during two main processes, gelatinization and retrogration.

Gelatinization occurs when starch granules and water are heated or sheared with significant energy to cause irreversible swelling of the granule (quantified by scanning electron microscopy (SEM) and small-angle X-ray scattering (SAXS)), loss of birefringence (polarized light microscopy), leaching of amylose and possibly amylopectin from the granule (chromatography), loss of double helical structure (NMR), loss of

crystallinity (X-ray diffraction), and an endothermic melting or dissociation event (differential scanning calorimetry, DSC) (*1*). Once the cooling of gelatinized starch begins, the process of retrogradation also begins because the resultant starch gel exists in a metastable, nonequilibrium state.

Retrogradation is a dynamic process involving the making and breaking of molecular level interactions between starch and water molecules. During retrogradation, the starch gel undergoes structural transformations (e.g., chain aggregation or recrystallization) resulting in a change from an initially amorphous state to a more ordered or crystalline state (*2, 3*). These molecular interactions exhibit molecular level consequences, such as changes in the molecular mobility of starch and water, as well as macroscopic consequences, such as textural changes (i.e., gel thickening and water loss). It has been suggested that the process of retrogradation can be viewed as a temperature-dependent three step sequential mechanism of nucleation, propagation, and maturation (*4, 5*). Using rheology and DSC, starch gels were observed to retrograde faster at low temperatures indicating that retrogradation follows nucleation type kinetics (*2, 6*). Several methods have been used to study starch retrogradation and have recently been reviewed by Karim et al. (*7*).

---

* To whom correspondence should be addressed. Tel: (217)333-6369. Fax: (217)244-7877. E-mail: sjs@uiuc.edu.
  † General Mills.
  ‡ Department of Food Science and Human Nutrition, University of Illinois.
  § Purdue University.
  || VOICE NMR Lab, University of Illinois.

Despite the vast amount of research done on gelatinization and retrogradation of starches (*8*), many features of these events are still incompletely understood at the molecular level (*9*). Moreover, retrogradation in low starch concentration gels (<20%) is difficult to measure by either conventional methods, such as DSC (*7*), or existing solid NMR techniques, such as magic angle spinning (MAS) NMR, because of the low amount of solids.

Low starch concentrations are used in a wide variety of food products, such as salad dressings, gravy mixes, and condiments. Perhaps, a better understanding of these low solid starch systems could be gained by collectively relating the results of multiple techniques performed on the desired system that are capable of measuring different aspects of the system, such as observing changes in the solid vs liquid phases or the dynamic vs structural or the macro- to mesoscopic vs molecular properties. Therefore, the objective of this research is to measure and compare the various properties of starch retrogradation in low solid systems using rheology, DSC, and an array of NMR spectroscopy techniques, including an improved cross-relaxation spectroscopy (CRS) technique and model.

EXPERIMENTAL PROCEDURES

Sample Preparation. Pure food powder starch (dent corn starch) provided by Staley Manufacturing Co. (Decatur, IL) contained 9.5% water as determined by vacuum oven drying at 100 °C for 5 h. The starch was mixed with a 0.05% solution of potassium sorbate (for the prevention of mold growth) in deionized ultrapure water to make four starch slurries of 5, 10, 15, and 25% starch by dry weight of starch on a total weight basis (dry weight of starch/(dry weight of starch + weight of water) × 100). These samples were hydrated for at least 12 h to allow the starch/water suspension to reach equilibrium before gelatinization. Because of differences in sample presentation requirements, it was necessary to develop individual starch gelatinzation procedures for each technique. The conditions of gelatinization for each technique were kept as similar as possible to minimize any possible sample differences and are described below. After gelatinization, all samples were aged at room temperature, 23 ± 1 °C.

DSC. DSC was performed on a DSC7 (PerkinElmer Instruments, Norwalk, CT) calibrated with indium, controlled by the Pyris Thermal Analysis Manager (version 3.72), and equipped with the nitrogen-flushed robotic RSe system. The flow rate for the N_2 carrier gas was 20 mL/min. Starch suspensions of 28.5 ± 1.50 mg were transferred to preweighed stainless steel sample pans, weighed, hermetically sealed, and reweighed. An empty pan of similar weight (±0.5 mg) to the sample pan was used as the reference pan for all samples.

Immediately after sealing, the starch slurry was gelatinized in the DSC using a heating rate of 10 °C/min from 25 to 100 °C and cooled to 25 °C at a rate of 15 °C/min. The change in enthalpy (ΔH_g) and the onset T_o, peak T_p, and final T_f temperatures for gelatinization were obtained from the gelatinization DSC endotherm. The starch gels were aged at room temperature and monitored for retrogradation at day 3, 8, 16, 21, 28, and 34. The retrogradation experiments were conducted at a heating rate of 10 °C/min over the temperature range of 25−110 °C. The change in enthalpy (ΔH_r) and the onset T_o, peak T_p, and final T_f temperatures for retrogradation were obtained from the retrogradation DSC endotherm. The six retrogradation measurement times over the 34 day period were done in duplicate for each concentration, and the average results along with their standard deviations were calculated.

Small Amplitude Oscillatory Shear Stress Rheology. The starch slurry was gelatinized at 92 °C for 10 min in a screw cap culture tube submerged in a 92 °C water bath with occasional venting. The starch slurry was transferred to a 25 mm parallel plate rheometer preheated to 90 °C with the gap set to 1.050 mm and cooled to 25 °C in about 10 min. The excess gel was trimmed after it was cooled to 25 °C to allow for shrinkage of the starch gel upon cooling. The gap was then narrowed to 1.000 mm. To inhibit evaporation, the top plate was covered with a high melting point mineral oil.

Starch retrogradation was monitored with a small amplitude oscillatory shear stress Ares rheometer (Rheometric Scientific, Inc., Piscataway, NJ). All measurements were performed at a constant temperature of 25 °C with data collection every 20 min for 48 h at 0.2 Hz and 2% strain. Unfortunately, it was not logistically possible to collect data longer than 48 h. In all cases, testing indicated that G' at 0.2 Hz and 2% strain was found to be within the linear viscoelastic region for the starch gels and independent of the frequency and strain. At least two samples of each concentration were analyzed, and the average results along with their standard deviations were calculated.

NMR Spectroscopy. The following procedure was used to prepare the starch gels for the NMR studies: (i) an empty 5 mm NMR tube was preheated to 92 °C by partially submerging the tube in a water bath, (ii) ~0.7 mL of the starch slurry was injected into the partially submerged NMR tube using a 1 mL syringe with an 8 in. needle with a flat end, (iii) the sample was heated for 3 min, and (iv) the sample was removed from the water bath and air-cooled to room temperature. All NMR experiments were performed in duplicate at 25 °C with no spinning. The specific NMR parameter was then obtained as described under each experiment, and the individual and average standard deviation were calculated.

Oxygen-17 (^{17}O) T_1 and T_2. A Varian UNITY INOVA 500 NMR (Palo Alto, CA) equipped with a 5 mm HPX (proton detect with ^{17}O tuned to the X channel) probe was used to obtain the ^{17}O T_1 and T_2 data at 68 MHz. The ^{17}O T_1 data were acquired with an inversion recovery (IR) pulse sequence (*10*) using the following parameters: relaxation delay time of 50 ms; 90° and 180° pulse width of 18.5 and 37 μs, respectively; eight delay times (τ) ranging from 0.1 to 20 ms; sweep width of 40 kHz; 98 scans; acquisition time of 0.1 s; and data size of 8k with zero filling to 16k. T_1 was calculated using the Varian fitting program "t1", where the ^{17}O peak intensity at each τ was plotted according to eq 1:

$$\ln(M_0 - M_z(t)) = \ln2 \cdot M_0 - \tau/T_1 \qquad (1)$$

where M_0 is the maximum signal intensity (at $t = 0$) and $M_z(t)$ is the signal intensity at time $t = \tau$. The individual T_1 standard deviations ranged from ±0.12 to ±0.51, and the average T_1 standard deviation was ±0.26.

The ^{17}O T_2 data were acquired using a single 90° pulse with a 3 kHz proton decoupling pulse applied at 500 MHz from the 90° pulse through acquisition, using the following parameter: relaxation delay time of 50 ms; 90° pulse width of 18.5 μs; sweep width of 40 kHz; 512 scans; acquisition time of 0.1 s; and data size of 8k with zero filling to 16k. The line width at half-height $\Delta\nu_{1/2}$, obtained by the Varian macro "res", was used to calculate T_2 via eq 2:

$$T_2 = \frac{1}{\pi\Delta\nu_{1/2}} \qquad (2)$$

The individual T_2 standard deviations ranged from ±0.01 to ±0.19, and the average T_2 standard deviation was ±0.05.

Proton (^1H) Diffusion Coefficient. A Varian UNITY INOVA 500 NMR equipped with a 5 mm HPX (proton detect with ^{17}O tuned to the X channel) probe was used to obtain the ^1H diffusion data at 500 MHz. The ^1H diffusion data were acquired with a Pulsed Field Gradient Stimulated Echo (PFGStE) experiment (*11*, *12*) using the following parameters in the pulse sequence (**Figure 1A**): relaxation delay time (d1) of 13 s; the length of the gradient pulse (g1) of 1 ms; d2 of 10 ms, which is the delay between the first and the second 90° pulses minus g1 and the delay between the third 90° pulses and acquisition minus g1; d5 of 60 ms, which is the delay between the second and the third 90° pulses; 90° pulse of 6.5−7.0 μs; amplitude of the gradient pulse was increased from 0.60 to 60 G/cm in eight logarithmically spaced steps; spectral width of 2 kHz; four scans; acquisition time of 0.512 s; and data size of 2k with zero filling to 4k. The diffusion coefficient (D_0) was calculated using the Varian macro, "pge_process". The individual D_0 standard deviations ranged from ±0.03 to ±0.11, and the average D_0 standard deviation was ±0.07.

Proton (^1H) CRS. A Varian UNITY INOVA 600 NMR spectrometer equipped with a 5 mm HCN triple axis gradient probe was used to
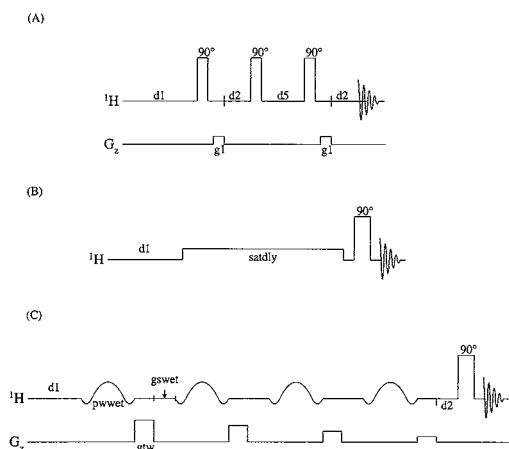
Figure 1. **(A)** PFGStE pulse sequence where ^1H is the proton channel; G_z is the gradient along the z-axis; d1 is the relaxation delay time of 13 s; g1 is the length of the gradient pulse of 1 ms; a d2 of 10 ms is the delay between the first and the second 90° pulses minus g1 and the delay between the third 90° pulses and acquisition minus g1; a d5 of 60 ms is the delay between the second and the third 90° pulses; and a 90° pulse of 6.5–7.0 μs was used. **(B)** The CRS pulse sequence where the experiment is performed on the ^1H channel, d1 is the relaxation delay time between successive pulses, and satdly is the length of the saturation pulse. The strength of the saturation pulse is ω_1 and is applied at a frequency that is offset from the liquid signal by a frequency Δ. **(C)** The saturation recovery pulse sequence with a "wet" pulse. The ^1H channel was used for the application of the proton pulses, while a gradient along the z-axis was applied on the G_z channel. The delay parameters are d1 = 2 s, pwwet = 4.75 ms, gswet = 2 ms, gtw = 2 ms, and d2 = 0.001– 15 s.

collect ^1H CRS data using CRS experiments at 600 MHz. The CRS pulse sequence is presented in **Figure 1B**. The CRS experiment was performed using 24–27 logarithmically spaced off resonance irradiation values Δ from 0.014 to 213 kHz and five (2200, 1210, 660, 366, and 111 Hz) to six (2200, 1210, 660, 366, 201, and 111 Hz) irradiation power levels ω_1. Because retrogradation occurs at a faster rate during the first 24 h (13), the minimum number of Δ and ω_1 values was used to obtain the initial (<24 h) CR data because it reduced the collection time by 5.6 min so changes in the sample that occur due to retrogradation will be on a different time scale than used for measuring the sample, i.e., the time required to collect the data will not influence the results. A saturation pulse length (satdly) of 7 s was needed to achieve steady state. The remaining parameters were as follows: relaxation delay time (d1) of 1 s; 90° pulse width of 8.2–8.5; sweep width of 4.2 kHz; 1 scan; acquisition time of 0.512 s; and data size of 4k with zero filling to 8k. More information regarding appropriate selection of CRS parameters is given by Lewen (14) and Lewen et al. (15). Phase cycling can be used to remove any residual transverse magnetization following off-resonance irradiation. However, it was determined that phase cycling did not significantly improve the CR data for this study.

The cross-relaxation data were analyzed using the method presented in the Cross-Relaxation Data Fitting section. However, instead of using the intensity of each peak as previous studies have done (16–18), the baseline-corrected integrated area of each peak was used because the water peak broadened depending on the conditions used for the experiment, possibly due to inhomogeneities in the sample and instrument. For more information about CRS, see the following references (13–27).

Proton (^1H) T_1. A Varian UNITY INOVA 600 NMR spectrometer equipped with a 5 mm HCN triple axis gradient probe was used to collect the ^1H T_1 data using a saturation recovery experiment at 600 MHz. The ^1H T_1 data were used in the fitting of the cross-relaxation data as R_A^{obs} (see Cross-Relaxation Data Fitting section). The saturation recovery pulse sequence (28) is presented in **Figure 1C**, using the

following parameters: relaxation delay time (d1) of 2s; the length of the wet pulse (pwwet) of 4.75 ms with a power level (wetpwr) of 16; length of the gradient pulse (gtw) of 2 ms with a power level that decreases with successive applications starting at a gradient strength (gzlvlw) of 65 G/cm; length of the delay between the gradient pulse and the wet pulse (gswet) of 2 ms; length of the delay between the last gradient pulse and the 90° pulse (d2) of 0.001–15 s; 90° pulse width of 8.2–8.5 μs; sweep width of 4.2k; 1 scan; acquisition time of 0.512 s; data size of 4k with zero filling to 8k. T_1 was calculated by fitting the integrated areas of the resulting peaks to eq 1 using the Varian macro t1.

Cross-Relaxation Data Fitting. The Henkelman model (16–18) was used to analyze the CR data. The model consists of two pools, a liquid pool (A) and a semisolid pool (B), in which each pool has an independent longitudinal relaxation rate, R_A and R_B (where $R = 1/T_1$) and an independent transverse relaxation time, T_{2A} and T_{2B}. Upon selective saturation by off-resonance irradiation of the longitudinal magnetization of the semisolid pool, some longitudinal magnetization in each pool is lost at rates of R_{RFA} and R_{RFB}:

$$R_{RFA} = \omega_1^2 \pi g_A(2\pi\Delta) \text{ and } R_{RFB} = \omega_1^2 \pi g_B(2\pi\Delta) \qquad (3)$$

where ω_1 is the irradiation power level in rad/s, Δ is the offset frequency of the irradiation pulse in Hz, and $g_A (2\pi\Delta)$ and $g_B (2\pi\Delta)$ are the absorption line shapes for the spins in each pool. Three commonly used line shape functions are

$$\text{Lorentzian: } g(2\pi\Delta) = \frac{T_2}{\pi} \frac{1}{[1 + (2\pi\Delta T_2)^2]} \qquad (4)$$

$$\text{Gaussian: } g(2\pi\Delta) = \frac{T_2}{\sqrt{2\pi}} e^{-(2\pi\Delta T_2)^2/2} \qquad (5)$$

superLorentzian: $g(2\pi\Delta) =$

$$\int_0^{\pi/2} \sin\theta \sqrt{\frac{2}{\pi}} \frac{T_2}{|3\cos^2\theta - 1|} e^{-2(2\pi\Delta T_2/|3\cos^2\theta - 1|)^2} d\theta \quad (6)$$

where θ is the angle between the external magnetic field and the projection of the dipolar interactions along the symmetry axis of motion (see Morrison and Henkelman (17) and Li et al. (18) for a detailed explanation).

The transfer rate of magnetization between the two pools is characterized by a fundamental rate constant, R. The concentrations of both pools, M_0^A and M_0^B, remain constant in size. Thus, the rate of magnetization transfer in either direction is a second-order rate constant given by $RM_0^A M_0^B$, which is reduced to RM_0^B because M_0^A is normalized to 1. At steady state, the modified Bloch derivatives for the two pool model can be solved for the z magnetization component of the liquid pool, M_z^A.

By noting that $(2\pi\Delta T_{2A})^2 \gg 1$ for all significantly nonzero points and using the Lorentzian line shape function (eq 4) to describe the liquid pool line shape (R_{RFA}), the z magnetization component of the liquid pool, M_z^A, can be given as

$$M_z^A = \frac{R_B\left[\dfrac{RM_0^B}{R_A}\right] + R_{RFB} + R_B + R}{\left[\dfrac{RM_0^B}{R_A}\right](R_B + R_{RFB}) + \left(1 + \left(\dfrac{\omega_1}{2\pi\Delta}\right)^2\left[\dfrac{1}{R_A T_{2A}}\right]\right)(R_B + R_{RFB} + R)}$$

(7)

For this work, it was found that the superLorentzian line shape (eq 6) provided the best fit for the gelatinized starch data and was used exclusively. The superLorentzian line shape is expected to arise from partially ordered materials (17), such as retrograded starch.

The experimental data were fit to the model (eqs 6 and 7) using the "lsqcurvefit" function from the optimization toolbox of the MATLAB (The MathWorks Inc, Natick MA) software package. The function

lsqcurvefit solves nonlinear data fitting equations using the least-squares method with the implementation of the Levenberg–Marquardt method. The integral of the superLorentzian was evaluated numerically with a step size of $d\theta$ sufficiently small to avoid numerical errors. Typically, 25 steps were used to evaluate $d\theta$ and the area of the integral region was calculated using Simpson's approximation.

Unique sets of model parameters (R_A, T_{2A}, R_B, R, M_0^B, and T_{2B} [via R_{RFB}]) cannot be determined by fitting the experimental data to eq 7 because the steady state experiments do not contain explicit reference to absolute time scales (*29*). As discussed by Henkelman et al. (*16*) and Li et al. (*18*), R_B cannot be reliably determined from the fit and was set to 1 s^{-1}. Therefore, four model parameters (R, RM_0^B/R_A, $1/(R_A T_{2A})$, and T_{2B}) were able to be determined with reasonable accuracy by fitting the data to eq 7 with $R_B = 1$ s^{-1}. Although the "absolute" values cannot be determined for the model parameters by fitting of the cross-relaxation data because R_B is set and not determined, the trends over time for each parameter should not change with a change in R_B.

Fitting the cross-relaxation data to eq 7 results in the best fit values for the parameter groups R, RM_0^B/R_A, $1/(R_A T_{2A})$, and T_{2B}. To determine the values for the individual parameters R_A, M_0^B, and T_{2B}, the following method was used. The first step was to determine R_A, the longitudinal relaxation rate that is independent of the interference of pool B. R_A was determined using eq 8 using the best fit parameter groups from eq 7:

$$R_A = \frac{R_A^{obs}}{1 + \left(\frac{\left[\frac{RM_0^B}{R_A} \right] (R_B - R_A^{obs})}{(R_B - R_A^{obs}) + R} \right)} \quad (8)$$

where the observed longitudinal relaxation rate R_A^{obs} is measured using the saturation recovery experiment described previously (see Proton (^{1}H) T_1). The other individual parameters were determined by substituting R_A back into the parameter groups, RM_0^B/R_A and $1/(R_A T_{2A})$ from the best fit to the CR data.

The validity of the fit was evaluated based on the average residual deviation per point (ARD) between the fit and the experimental data. Equation 9 is the formula for ARD:

$$ARD = \sqrt{\frac{\sum_{i=1}^{N} (fit_i - data_i)^2}{N}} \cdot 100 \quad (9)$$

where N is the number of data points.

The confidence limits of the fitted parameters were determined by finding the maximum and the minimum values of a parameter while setting all remaining parameters to their optimized values such that:

$$\chi^2 = \chi_0^2 \left[1 + \frac{n}{N - n} F(n, N - n, p) \right] \quad (10)$$

where n is the number of fitted parameters (4), N is the number of data points, p is the desired confidence level (set to 90% for this work), F is the F distribution function, χ_0^2 is χ^2 determined with the optimized parameters, and χ^2 is defined as:

$$\chi^2 = \frac{1}{N - n - 1} \sum_{i=1}^{N} \frac{(fit_i - data_i)^2}{\sigma^2} \quad (11)$$

where σ is the measurement reproducibility error of each data point (*30, 31*). Substituting eq 11 into eq 10 results in the following solvable equation:

$$\sum_{i=1}^{N} (fit_i - data_i)^2 =$$
$$\sum_{i=1}^{N} (fitOpt_i - data_i)^2 \left[1 + \frac{n}{N - n} F(n, N - n, p) \right] \quad (12)$$

where fitOpt is the fit solution determined with the optimized parameters.

RESULTS

DSC. DSC was used to measure the enthalpy and temperature parameters associated with the gelatinization endotherm for the native starch granules. The gelatinization of four 5, 10, 15, and 25% starch concentrations resulted in a single concentration-independent endotherm with an average onset temperature $T_o = 65.9 \pm 0.08$ °C, peak temperature $T_p = 70.6 \pm 0.08$ °C, final temperature $T_f = 75.4 \pm 0.16$ °C, and gelatinization enthalpy $\Delta H_g = 17 \pm 1.2$ J/g (**Table 1**). These values are similar to those reported in the literature (**Table 2**).

DSC was also used to measure the enthalpy and temperature parameters associated with starch retrogradation by monitoring the progressively increasing endotherm due to recrystallization of amylopectin molecules with storage time (*32*). A measurable change in enthalpy for retrogradation (ΔH_r) due to recrystallization of amylopectin occurred after 4 weeks of storage for the 15% starch gel and 1 week of storage for the 25% starch gel (**Figure 2**). The percent retrograded, as defined by Jane et al. (*33*), equals ΔH_r divided by ΔH_g multiplied by 100 and is also plotted in **Figure 3** and is discussed below. A gradual increase in ΔH_r occurred over the 34 day period for the 25% starch gel. No measurable retrogradation DSC endothermic peaks were detected for the 5 and 10% starch gels. The corresponding retrogradation transition temperatures and enthalpy for the 15 and 25% starch gels are reported in **Table 3**. The endothermic peak for the 25% starch gel broadens as a function of storage time; that is, T_o decreased and T_f increased.

The rate and extent of retrogradation is a function of many parameters, including starch concentration, starch type/composition, gelatinization conditions, storage temperature and time, which makes it difficult to compare results to literature values as illustrated in **Figure 3**. **Figure 3** is a collection of the DSC results reported by several researchers studying the retrogradation of dent corn starch under various conditions. The importance of **Figure 3** is to illustrate how different retrogradation results (i.e., rate and extent of retrogradation) can be obtained under seemingly similar conditions. For example, Baker and Rayas-Duarte (*37*) and Paredes-Lopez et al. (*38*) reported retrogradation data for a 30% dent corn starch gel stored at 4 °C. However, the starch gel of Baker and Rayas-Duarte (*37*) retrograded at a faster rate than the starch gel of Paredes-Lopez et al. (*38*).

However, the qualitative results of these studies are the same. These studies show that the rate and extent of retrogradation of amylopectin depend on the concentration of starch and storage temperature. An optimal concentration for the recrystallization of amylopectin was found to be 50–60% for wheat starch (equivalent to 37.5–45% amylopectin) stored at 25 °C for 7 days (*40*). Very little crystallinity was observed for dilute starch gels (<20% starch). It is widely reported that a starch concentration of 20% is required to study retrogradation with DSC (*7, 40–42*).

The retrogradation results obtained in this study occurred at a slower rate as compared to those reported in the literature. However, these results are supported by the NMR data (see

Table 1. Gelatinization Endotherm Temperatures (T_o, T_p, $T_f \pm$ SD) and Enthalpy Values ($\Delta H_g \pm$ SD) for 5, 10, 15, and 25% Dent Corn Starch Samples

% starch	N^a	T_o (°C)	T_p (°C)	T_f (°C)	ΔH_g (J/g)^a
5	10	65.7 ± 0.22	70.4 ± 0.03	74.9 ± 0.06	13 ± 2.8
10	10	66.0 ± 0.07	71.2 ± 0.13	76.0 ± 0.08	21 ± 3.8
15	12	66.1 ± 0.18	70.8 ± 0.06	74.7 ± 0.10	18 ± 1.6
25	12	65.6 ± 0.14	70.0 ± 0.11	76.0 ± 0.41	16 ± 1.2
overall	44	65.9 ± 0.08	70.6 ± 0.08	75.4 ± 0.16	17 ± 1.2

^{a} N = the number of samples, and ΔH_g is J/g on a dry basis.

Table 2. Gelatinization Endotherm Temperatures and Enthalpy Values for Dent Corn Starch Samples Obtained from the Literature^a

| ref no.	% starch	T_o (°C)	T_p (°C)	T_f (°C)	ΔH_g (J/g)
34	20	NA	70.8	NA	9.8
35	25	NA	70.2	NA	14.3
36	25	66.5	NA	NA	13.2
33	25	64.1	69.4	75.9	12.3
37	30	66.2	70.3	NA	8.3
38	35	65	71.2	82	14.5
36	35	65.5	NA	NA	13.5
39	68	NA	72	NA	13.4

^{a} NA = not available because the authors did not provide this information.
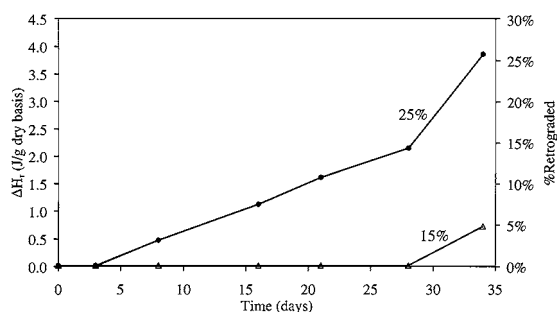
Figure 2. Change in ΔH_r (primary *y*-axis) and the corresponding percent retrograded values (secondary *y*-axis) over time for the 15 (△) and 25% (●) starch samples.

NMR Spectroscopy section). As expected, very little to no crystallinity was measured for the dilute (<20%) starch gels. In fact, the only crystallinity observed for the dilute samples was for the 15% starch gel after 34 days of aging.

Rheology. Rheology detects the structural development of the full three-dimensional polymer network of a system. **Figure 4** shows the development of G' for the starch gels over a 48 h period. A biphasic retrogradation process was observed for the 25% starch gel in which an initial (0−3 h) rapid rise in G' is followed by a much slower development of G' over the 48 h period, whereas only an initial (0−3 h) rapid rise in G' was observed for the more dilute (≤15%) starch gel samples. In addition, a greater value for G' was observed at higher starch concentrations as compared to lower concentrations.

Biliaderis and Zawistowski (*6*) observed a similar biphasic retrogradation process during the first 20 h of storage for wheat starch gels (concentration ≥ 20%). The initial rapid rise in the development of G' is attributed to the rapid establishment of a three-dimensional amylose network caused by interchain associations in the polymer rich phase of the sample (i.e., formation of amylose double helical structures), followed by the establishment of junction zones via the slower processes of cross-linking and annealing resulting in an increase of amylose crystallinity at concentrations above the critical gelling con-
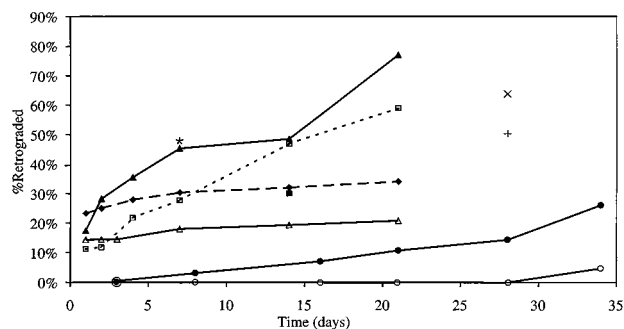
Figure 3. Collection of the DSC results reported by several researchers studying the retrogradation of dent corn starch under various conditions as a comparison to the data obtained in this study. Reference, symbol, temperature, and concentration: present study (○), 23 °C and 15%; Mua and Jackson (*34*) (■), 4 °C and 20%; Jane et al. (*33*) (×), 4 °C and 25%; present study (●), 23 °C and 25%; Ward et al. (*36*) (+), 23 °C and 25%; Baker and Rayas-Duarte (*37*) (◆), −20 °C and 30%; Baker and Rayas-Duarte (*37*) (▲), 4 °C and 30%; Baker and Rayas-Duarte (*37*) (□), 25 °C and 30%; Paredes-Lopez et al. (*38*) (△), 4 °C and 30%; Ward et al. (*36*) (*), 23 °C and 35%.

Table 3. Retrogradation Endotherm Temperatures (± SD) and Enthalpy Values ($\Delta H_r \pm$ SD) for the 15 and 25% Dent Corn Starch Samples

% starch	time (days)	T_o (°C)	T_p (°C)	T_f (°C)	ΔH_r (J/g)
15	0−28	0 ± 0	0 ± 0	0 ± 0	0 ± 0
15	34	55.0 ± 0.22	60.7 ± 0.33	66.3 ± 0.46	0.84 ± 0.04
25	3	0 ± 0	0 ± 0	0 ± 0	0 ± 0
25	8	55.1 ± 0.01	60.0 ± 0.00	63.6 ± 0.17	0.47 ± 0.00
25	16	55.1 ± 0.01	60.6 ± 0.25	66.7 ± 0.90	1.3 ± 0.42
25	21	55.1 ± 0.08	61.6 ± 0.42	67.5 ± 0.48	1.7 ± 0.14
25	28	55.5 ± 0.10	61.7 ± 0.00	67.2 ± 0.08	2.2 ± 0.16
25	34	53.2 ± 0.20	61.4 ± 0.17	68.6 ± 0.45	3.9 ± 0.34
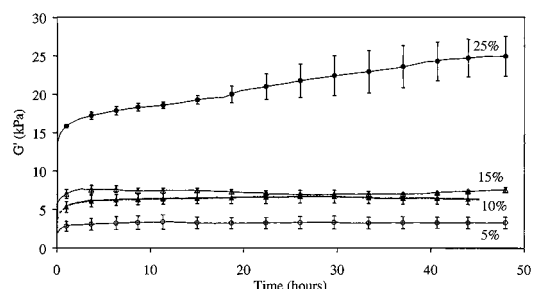
Figure 4. Plot of G' (kPa) of 5 (○), 10 (▲), 15 (△), and 25% (●) starch samples over a 48 h period after gelatinization. The error bars represent the standard deviation.

centration for amylose, $C_o \sim 1.0\%$ (*8*, *43−47*). Cross-linking, the creation of junction zones from the association of interchain double helices, determines the critical gelling concentration (not molecular entanglement) and impedes the growth of crystalline arrays of double helices (*45*). The final amylose gels consist of three interconnected regions: (i) amorphous (DP ≈ 9−20), (ii) crystalline (DP ≈ 23−52), and (iii) intermediary (DP ≈ 3−6), in which the amylose chains are long enough to participate in the different regions (*48*).

On the other hand, the slower development of G' is linked to amylopectin and is attributed to the two step amylopectin network formation: (i) the initial formation of the amylopectin aggregates due to double helical associations of the amylopectin branches followed by (ii) the intermolecular crystallization of the outer branches of amylopectin (*6*, *49*, *50*). In addition, the

critical overlap concentration $C*$ for amylopectin is 0.9% (8), while the formation of a stable amylopectin gel did not occur until amylopectin chains are heavily entangled at concentrations ≥10% (8, 49).

By using the approximation that dent corn starch contains ∼25% amylose and ∼75% amylopectin (8, 51), the 5, 10, 15, and 25% dent corn starch gels under investigation contain ∼1.25, 2.50, 3.75, and 6.25% amylose and 3.75, 7.50, 11.25, and 18.75% amylopectin, respectively. Therefore, the amount of amylose present for all four starch samples is greater than the critical gelling concentration required to form an amylose gel. The amylose gel formation is observed for each starch concentration as the initial increase in G' (**Figure 4**).

Both the 15 and the 25% starch gels contain over 10% amylopectin; however, only the 25% starch gel exhibited a biphasic retrogradation curve. The G' for the 5−15% starches did not increase over the 48 h period after the initial rapid increase in G' was complete within the first 3 h. Similarly, Biliaderis and Zawistowski (6) observed a biphasic increase in G' for wheat starch gels greater than 20% but not for the wheat starch gels less than 20% during the first 20 h of retrogradation at room temperature using a small oscillatory rheometer. However, studies with longer time frames have shown that G' increases gradually over days to weeks (32, 49).

NMR Spectroscopy. NMR spectroscopy is a noninvasive technique that can measure the structural and dynamic changes of liquid and solid components at the molecular level in situ. The effects of retrogradation on the water and starch components were monitored by water mobility (^{17}O T_1, ^{17}O T_2, and D_0) and CRS techniques, which probed both the liquid and the solid components of the starch gel system. To minimize the redundancies, the in depth analysis of the NMR results will be presented in the Discussion section.

Water Mobility Experiments. A single Lorentzian peak was observed for the ^{17}O T_1, ^{17}O T_2, and ^1H D_0 spectra at each concentration level and time period even though there are two fractions of water present, "bound" (or "associated") and "free". A rapid exchange between the two fractions of water results in a single Lorentzian peak that represents the average of both water fractions. Oxygen-17 NMR was used to measure the liquid longitudinal (T_1) and transverse (T_2) relaxation rates because proton-decoupled ^{17}O NMR is free of the complications of cross-relaxation and proton chemical exchange, which can be a problem with ^1H (proton) NMR (52, 53). The ^{17}O T_1 and T_2 time constants are related to the rotational and tumbling frequencies of the liquid molecules, i.e., T_1 and T_2 are a measure of the molecular mobility of the water in the starch gel matrix.

The T_1 time constant characterizes the rate at which excited nuclei dissipate excess energy to the lattice (environment). The dependence of T_1 on molecular mobility has a minimum at intermediate viscosities between the solid and the liquid states (54). As the concentration of starch increases from 5 to 25% starch, the ^{17}O T_1 values decrease nearly linearly from 6.4 to 4.0 ms for the initial measurements, respectively. However, no statistically significant change occurred over time for any of the starch gels as presented in **Figure 5A**.

T_2 characterizes the rate at which excited nuclei exchange energy or dephase. T_2 decreases with a reduction in the mobility of the molecule being measured (54). As the concentration of starch increases from 5 to 25% starch, the ^{17}O T_2 values decrease nearly linearly from 5.17 to 2.45 ms for the initial measurements, respectively. For all concentrations, there was a directional decrease in ^{17}O T_2 within the first couple of hours of aging as shown in **Figure 5B**, which may correspond with the formation
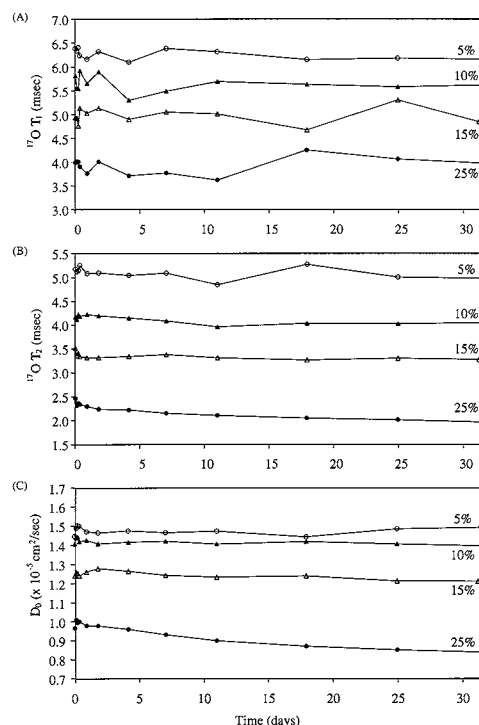

Figure 5. Plots of ^{17}O T_1 (**A**), ^{17}O T_2 (**B**), and D_0 (**C**) for the 5 (○), 10 (▲), 15 (△), and 25% (●) starch samples over a 31 day period after gelatinization.

of an amylose gel matrix that was observed using rheology. However, only the 25% starch concentration exhibited a continuous, statistically significant decrease from 2.45 to 1.96 ms in ^{17}O T_2 over the 31 day storage period, which corresponds to the retrogradation of amylopectin.

The ^{17}O T_2 values obtained for the initial gelatinized starch solutions reported here are similar to those reported by Chinachoti et al. (52) (1.0 ms for a 40% wheat starch solution in D_2O at 25 °C) and Cheetam and Tao (55) (3.5, 1.3, 1.2, and 0.9 ms for 17, 33, 40, and 50% maize starch solutions in D_2O, respectively, at 25 °C).

The rate of ^1H diffusion coefficient, D_0, is a measure of the translational motion of the water molecules. The diffusion results are presented in **Figure 5C**. As the concentration of starch increased from 5 to 25% starch, the D_0 values decreased nearly linearly from 1.5 to 1.0 × 10^{-5} cm²/s, respectively. No significant changes occurred over time for the 5−15% starch gels. However, a statistically significant decrease (at a 95% significance level) in D_0 from 1.0 to 0.8 × 10^{-5} cm²/s was observed for the 25% starch gel during the 31 day storage period.

Cross-Relaxation Experiments. CRS allows for the observation of the solid mobility, which is otherwise unobservable at the relatively low starch concentrations used in this study, and the ability to monitor the liquid properties independent of the interference from the solid. An explanation of how the cross-relaxation analysis was performed is presented in the Cross-Relaxation Data Fitting section. The fitted parameters that will be presented are the rate of magnetization transfer R, the solid transverse relaxation time constant T_{2B}, the liquid longitudinal relaxation time constant T_{1A}, the liquid transverse relaxation time constant T_{2A}, and the number of solid protons that participate in cross-relaxation M_0^B.

The rate of magnetization transfer measured by R is independent of concentration (16). Changes in R are observed for different heterogeneous systems, i.e., differences in R occur
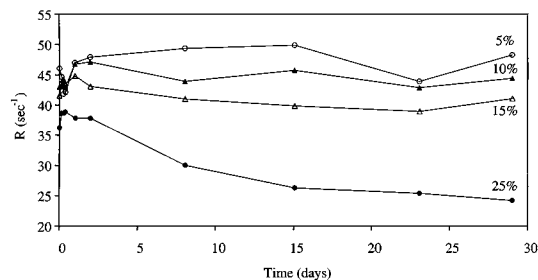
Figure 6. Plot of *R* for the 5 (○), 10 (▲), 15 (△), and 25% (●) starch samples over a 29 day period after gelatinization.
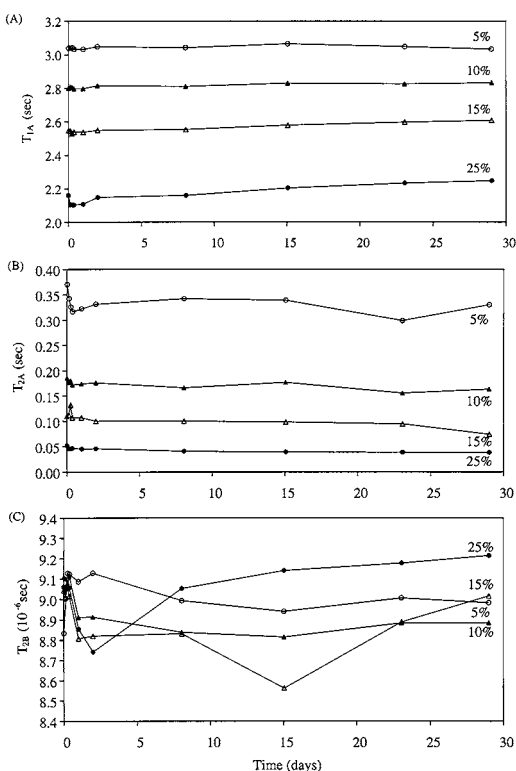

Figure 7. Plots of T_{1A} (**A**), T_{2A} (**B**), and T_{2B} (**C**) for the 5 (○), 10 (▲), 15 (△), and 25% (●) starch samples over a 29 day period after gelatinization.

between gel systems because of a difference in their structure. The results for *R* are presented in **Figure 6**. There was a high degree of variability in determining *R* (average SD ± 4.75). There was no statistical difference between any of the *R* values at two standard deviations. However, there is a directional decrease in *R* as the starch concentration increases from 5 to 25%, suggesting a possible change in gel structure with increasing starch concentration. Only the *R* value for the 25% starch sample gradually decreases over time, which suggests that a change in the gel structure is occurring during the retrogradation process.

The values for the liquid longitudinal relaxation time constant T_{1A} decreased from 3.04 to 2.16 s for the initial measurements of the 5−25% starch gels, respectively, and are presented in **Figure 7A**. In addition, no significant changes in T_{1A} were observed over time. These results are directionally similar to the ^{17}O T_1 results (**Figure 5A**).

The values for the liquid transverse time constant T_{2A}, presented in **Figure 7B**, show that there is a decrease from 0.37 to 0.05 s for the initial measurements with an increase in starch concentration from 5 to 25%, respectively. In addition, there is a decreasing trend in T_{2A} for each starch gel over the 29 day storage period. This is the first indication, for the experiments
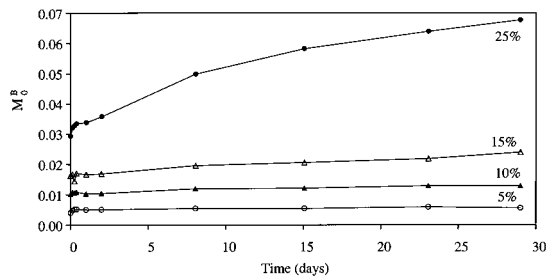

Figure 8. Plot of M_0^B for the 5 (○), 10 (▲), 15 (△), and 25% (●) starch samples over a 29 day period after gelatinization.

used in this study, that the mobility of the water might be changing over time for the starch concentrations ≤15%.

The values for the solid transverse relaxation time constant T_{2B} did not statistically change with concentration or time, as shown in **Figure 7C**. This indicates that the mobility of the starch components did not significantly change with concentration or over time. However, there was an increase in *G′* with concentration and time for the 25% sample as measured by rheology. The difference between the T_{2B} and the *G′* results is addressed in the Discussion section.

The final parameter that was determined from the cross-relaxation model was the number of solid protons that participate in cross-relaxation M_0^B. The concentration of both the liquid and the solid pools, $M_0^{A,B}$, remains constant in size for any given cross-relaxation experiment. However, the ratio of M_0^A to M_0^B will change for different samples. Because M_0^A is normalized to 1, the changes will be expressed in M_0^B. The results for M_0^B are presented in **Figure 8**. As the concentration increases from 5 to 25%, the initial values for M_0^B increased from 0.0041 to 0.0293. In addition, as the starch gels aged over the 29 day period, the values for M_0^B increased for all starch gel concentrations.

DISCUSSION

When combined, the various experimental results obtained in this study form a picture of the events unfolding during retrogradation. In this section, the NMR results will be compared to and combined with the DSC and rheology results presented in earlier sections. An important point to keep in mind when comparing the results from these different techniques is that each technique probes different length and time scales and is thus sensitive to different elements and levels of structure, heterogeneity, and functionality. The results for this section are divided into concentration and retrogradation effects.

Concentration Effects. For the initial measurements (time ≤ 1 h), as the concentration of starch increases, statistically significant experimental observations were made as follows: (i) an increase in *G′*, indicating that the gel is becoming more solid in nature; (ii) a decrease in ^{17}O T_1, ^{17}O T_2, D_0, T_{1A}, and T_{2A}, indicating a decrease in the molecular mobility of the water; (iii) an increase in M_0^B, indicating an increase in the number of solid protons that participate in cross-relaxation; (iv) no change in T_{2B}, indicating that the mobility of the solid molecules does not change with concentration; and (v) no change in *R*, indicating that the gel structures are similar.

The relationship between M_0^B and starch concentration was explored by plotting M_0^B and starch concentration (**Figure 9**). M_0^B was found to increase linearly with increasing starch concentration. The equation shown in **Figure 9** is valid only for the concentrations used in this experiment. More experiments
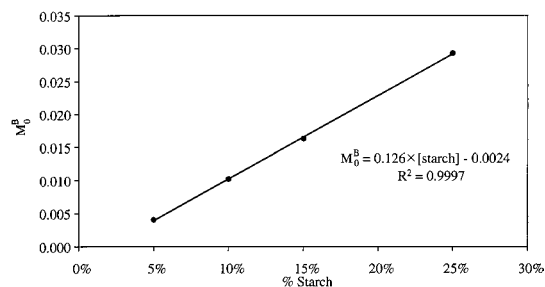
Starch Retrogradation

J. Agric. Food Chem., Vol. 51, No. 8, 2003 **2355**

Figure 9. Relationship of the initial M_0^B values to the concentration of the starch gel. A linear relationship between M_0^B and percent starch is observed.

would be required in order to determine the cross-relaxation dependence at lower and higher starch concentrations.

At first look, one would expect T_{2B} to increase with an increase in G' because an increase in rigidity is thought to be due to a decrease in solid mobility. However, the mobility of the solid does not change with an increase in G' according to the T_{2B} results reported here. So, what is the increase in solidlike character attributed to? The gel matrix can be viewed as a building. When the number of supports in the building are increased, the rigidity of the building increases because of the added supports. Within a gel structure, M_0^B increases over time (i.e., increase in the number of supports), which serves to increase the rigidity of the gel as observed by a decrease in G'. However, T_{2B} does not change because the "solidness" (mobility) of the solidlike protons does not change as the number of solidlike protons increases.

The results obtained for R support the above postulate for T_{2B}, G', and M_0^B because R is independent of concentration for similar heterogeneous systems. If R varied for each concentration, then, the gel structure for the different starch concentrations would be different. Therefore, as the starch concentration is increased, the gel structures between concentrations are similar (T_{2B} and R). An increase in the density of the gel matrix is observed by M_0^B, which in turn increases the rigidity of the matrix (G'). The mobility of the water decreased (^{17}O T_1, ^{17}O T_2, D_0, T_{1A}, and T_{2A}) with increasing starch concentration due to an increase in the ratio of bound to free water molecules and an increase in the density of the starch gel network.

Retrogradation Effects. The retrogradation of starch is a biphasic event attributed to the retrogradation of the amylose and amylopectin components as discussed in the DSC and Rheology sections. Therefore, the retrogradation effects can be divided into the amylose or fast (<24 h) component and the amylopectin or slow (>24 h) component. **Table 4** summarizes the results of the DSC, rheology, and NMR parameters for the retrogradation of the 25% starch gel. Changes observed in the 5−15% starch gel parameters are also noted in **Table 4**.

Only two of the measured parameters showed a statistically significant change over the initial 24 h of retrogradation. G' and M_0^B increased over the first 24 h of aging. A linear relationship between G' and M_0^B exists for the first 8 h of retrogradation (**Figure 10**), but the linear relationship between G' and M_0^B did not exist once amylopectin retrogradation began (>24 h). Therefore, during the retrogradation of amylose, the increase in the rigidity of the starch gel is accompanied by an increase in the number of solid molecules. The increase in M_0^B is a result of the conversion of the highly mobile starch fraction to the less mobile solid state due to the reassociation of the starch molecules during retrogradation. The other

Table 4. Results of the DSC, Rheology, and NMR Parameters for the Retrogration of a 25% Starch Gel over Time (Results Are Divided into Amylose and Amylopectin Components. Changes Observed in the 5–15% Starch Gel Parameters Are also Indicated As Explained in the Footnotes)

Amylose or Fast (<24 h) Component

rapid ↑ G' (<2.5–3.5 h) ⟹ gel is becoming more solid in nature[b]

rapid ↑ M_0^B (<8.5 h) ⟹ increase in the number of solid protons participating in cross-relaxation[b]

Amylopectin or Slow (>24 h) Component

↑ ΔH_r ⟹ increase in the amount of recrystallized amylopectin[a]

↑ G' ⟹ gel is becoming more solid in nature

↓ ^{17}O T_2, D_0, and T_{2A} ⟹ decrease in the molecular mobility of water[b]

↑ M_0^B ⟹ increase in the number of solid protons participating in cross-relaxation[b]

directional ↓ R ⟹ potential change in the molecular structure of the gel matrix

∅ T_{2B} ⟹ molecular mobility of solid molecules do not change[b]

∅ ^{17}O T_1 and T_{1A} ⟹ see text for explanation[b]

[a] Also observed for the 15% starch concentration. [b] Also observed for all of the starch concentrations.
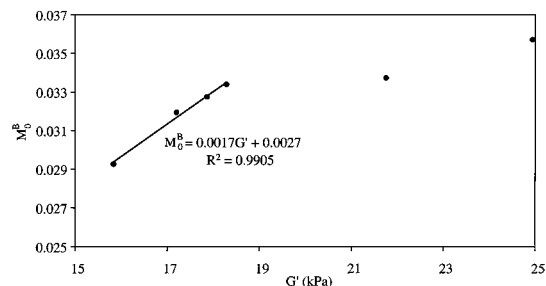

Figure 10. Relationship of M_0^B to G' (kPa) for the 25% starch gel over a 24 h period. During the retrogradation of amylose, a linear relationship between M_0^B and G' is observed.

measured parameters did not statistically change over the initial 24 h of retrogradation.

As discussed in the DSC section, the recrystallization of amylopectin is the dominant retrogradation process that occurs after aging the starch gel for more than 24 h. In addition to the increase in ΔH_r, the G' continued to increase for the 25% starch gel, while it ceased to increase for the 5−15% starch gels. A detailed discussion of the relationship between ΔH_r and G' is given by Biliaderis (8) and Lewen (14).

A decrease in the water mobility was observed using ^{17}O T_2, D_0, and T_{2A}. Also, there is an increase in M_0^B as a result of the conversion of the highly mobile starch fraction to the less mobile solid state due to the reassociation of the starch molecules during retrogradation (13). Ohtsuka et al. (56) observed a decrease in the distance between neighboring barriers with the aging of starch gels, i.e., the average size of the water compartments decreases over time. Therefore, a decrease in the mobility of water is observed due to a combination of an increase in the ratio of "bound" to "free" water molecules and an increase in molecular associations within the starch gel network over time.

Further supporting evidence that M_0^B is a measure of the recrystallization of amylopectin is provided by the comparison of percent retrograded to M_0^B, over the concentration range studied. A correlation of percent retrograded and M_0^B indicates that the increase in the crystallinity of amylopectin is proportional to the increase in the solid component, which consists of less mobile starch molecules. The resulting correlation is given in **Figure 11**.
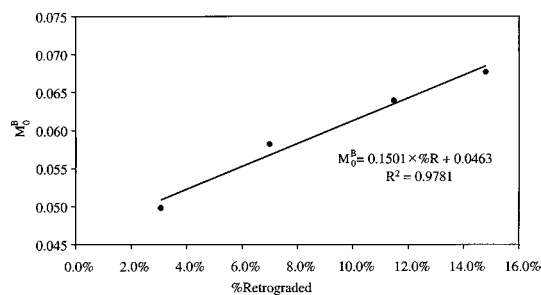
Figure 11. Relationship of M_0^B to percent retrograded as determined by DSC for the 25% starch gel over the 29 day storage period at 25 °C. During the retrogradation of amylopectin as determined by DSC, a linear relationship between M_0^B and percent retrograded is observed.

An interesting observation is that T_{2B} does not change over time. This result indicates that the mobility of the solid component does not change over time despite the conversion of the highly mobile starch fraction to the less mobile solid state during retrogradation. Therefore, T_{2B} does not change because the more mobile starch protons do not contribute to T_{2B} because they do not participate in cross-relaxation until they become less mobile.

The last results are the ^{17}O T_1 and T_{1A} measurements in which no statistically significant change is observed over time. T_2 values, obtained by the line width at half-height method (eq 2), observed at high solids concentrations, are often broadened by local magnetic fields due to varying environments in the sample (*10*). This results in smaller T_2 values as compared to T_1 values as observed in this study. Similar differences in T_1 and T_2 values (presented as R_1 and R_2^* values) were reported by Kou et al. (*57*) for instant dent corn starch using ^2H NMR.

Cross-relaxation experiments have been performed on waxy maize samples ranging from 10 to 45% solids (*13, 23*). In both papers, the area, intensity, and line width of the resulting CR spectra were analyzed to elucidate the underlying physical parameters of a different CR model than was used in the present study. It was postulated from the CR model that an increase in line width of the CR spectrum would correspond to a decrease in T_{2B} and an increase in the CR spectrum area corresponds to an increase in f (the ratio of solid to liquid protons, which is similar to M_0^B from the CR model used in the current study).

These authors analyzed the retrogradation of waxy maize starch gels stored at 5 °C up to 115 days. They observed an increase in both the line width and the area of the CR spectrum. Therefore, they hypothesized that there was a decrease in T_{2B} associated with the increase in line width and the increase in area was due to the increase in f.

In comparison to the present study of the retrogradation of maize starch stored at 23 °C up to 34 days, a decrease in T_{2B} was not observed, but an increase in M_0^B (similar to f) was observed in addition to a decrease in T_{2A}. Even though the line width of the CR spectra increases, a decrease in T_{2B} is not observed. Instead, T_{2B} remains constant because it is a measure of the solidlike component that participates in cross-relaxation. However, both the area from Eads studies (*13, 23*) and the M_0^B from the present study correlated to an increase in ΔH_r over time. More theoretical and experimental studies should be performed comparing the results of several different starches at various concentrations to further develop a relationship between the line width and the areas of a CR spectrum to their corresponding CR parameters.

The NMR methods used measure the average motion of the water within the starch, i.e., they cannot distinguish between bound and free water. It would be interesting to perform experiments capable of discerning between the bound and the free water and to determine if there is a wide range of water and starch mobilities within the system. Some advanced NMR techniques that may provide further insight into this area are a biexponential analysis of the CPMG relaxation curves (*58*) and diffusion-order spectroscopy (*59−61*).

CONCLUSION

Using DSC, rheology, and NMR, four concentrations of dent corn starch were studied in order to better understand the retrogradation of low solid systems by collectively relating multiple techniques that are capable of measuring different aspects of the system, such as observing changes in the solid vs liquid phases or the dynamic vs structural or the macro- to mesoscopic vs molecular properties. From this analysis, the retrogradation of dent corn starch can be divided into two components: (i) the amylose or fast (<24 h) component and (ii) the amylopectin or slow (>24 h) component.

During the initial (<24 h) stage of retrogradation, the amylose component reassociates faster than the amylopectin component. During this stage, the gel becomes more solid as observed by an increase in G'. This increase in G' corresponds to an increase in the number of solid protons measured by M_0^B using CRS. The changes in G' and M_0^B are observed for all four of the concentrations.

During the latter (>24 h) stage of retrogradation, amylopectin recrystallization becomes the dominant process. For the 25% starch gel, an increase in ΔH_r is observed with aging where ΔH_r corresponds to the amount of crystallized amylopectin in the starch gel. The increase in ΔH_r corresponds to an increase in M_0^B. In addition to the increase in M_0^B for the 25% starch gel, an increase in M_0^B was observed for the other tested starch concentrations. The other interesting measurement that was determined with CRS was that T_{2B} did not change over time or concentration. This result indicates that the mobility of the solid component does not change over time, despite the conversion of the highly mobile starch fraction to the less mobile solid state during retrogradation.

ACKNOWLEDGMENT

LITERATURE CITED

(1) Fisher, D. K.; Thompson, D. B. Retrogradation of Maize Starch After Thermal Treatment Within and Above the Gelatinization Temperature Range. *Cereal Chem.* **1997**, *74*, 344−351.

(2) Gudmundsson, M. Retrogradation of Starch and the Role of Its Components. *Thermochim. Acta* **1994**, *246*, 329−341.

(3) Parker, R.; Ring, S. G. Aspects of the Physical Chemistry of Starch. *J. Cereal Sci.* **2001**, *34*, 1−17.

(4) Levine, H.; Slade, L. Non-Equilibrium Behavior of Small Carbohydrate-Water Systems. *Pure Appl. Chem.* **1988**, *60*, 1841.

Starch Retrogradation

J. Agric. Food Chem., Vol. 51, No. 8, 2003 **2357**

(5) Levine, H.; Slade, L. Influence of Glassy and Rubbery States on the Thermal, Mechanical, and Structural Properties of Doughs and Baked Products. In *Dough Rheology and Baked Product Texture*; Fairidi, H., Faubion, J. M., Eds.; Van Nostrand Reinhold: New York, 1989; pp 157−300.

(6) Biliaderis, C. G.; Zawistowski, J. Viscoelastic Behavior of Aging Starch Gels: Effects of Concentration, Temperature, and Starch Hydrolysates on Network Properties. *Cereal Chem.* **1990**, *67*, 240−246.

(7) Karim, A. A.; Norziah, M. H.; Seow, C. C. Methods for the study of starch retrogradation. *Food Chem.* **2000**, *71*, 9−36.

(8) Biliaderis, C. G. Structures and Phase Transitions of Starch Polymers. In *Polysaccharide Association Structures in Food*; Walter, R. H., Ed.; Marcel Dekker: New York, 1998; pp 57−168.

(9) Appelqvist, I. A. M.; Martine, R. M. D. Starch − Biopolymer Interactions − A Review. *Food Rev. Int.* **1997**, *13*, 163−224.

(10) Derome, A. E. *Modern NMR Techniques for Chemistry Research*; Pergamon Press: Oxford, U.K., 1987.

(11) Tanner, J. E. Use of the Stimulated Echo in NMR Diffusion Studies. *J. Chem. Phys.* **1970**, *52*, 2523−2526.

(12) Price, W. S. Pulsed-Field Gradient Nuclear Magnetic Resonance as a Tool for Studying Translational Diffusion: Part 1. Basic Theory. *Concepts Magn. Res.* **1997**, *9*, 299−336.

(13) Wu, J. Y.; Eads, T. M. Evolution of Polymer Mobility during aging of Gelatinized Waxy Maize Starch: A Magnetization Transfer ^{1}H NMR Study. *Carbohydr. Polym.* **1993**, *20*, 51−60.

(14) Lewen, K. S. The Development and Application of Nuclear Magnetic Cross Relaxation Spectroscopy to Model and Retrograding Starch Systems. Ph. D., University of Illinois at Urbana-Champaign, 2000a.

(15) Lewen, K. S.; McCormick, I. H.; Molitor, P.; Schmidt, S. J.; Eads, T. M. Factors Affecting the Collection and Fitting of Nuclear Magnetic Cross Relaxation Spectroscopy Data with Application to Waxy Corn Starch. *J. Agric. Food Chem.* **2000b**, *48*, 4469−4476.

(16) Henkelman, R. M.; Huang, X.; Xiang, Q.-S.; Stanisz, G. J.; Swanson, S. D.; Bronskill, M. J. Quantitative Interpretation of Magnetization Transfer. *Magn. Reson. Med.* **1993**, *29*, 759−766.

(17) Morrison, C.; Henkelman, R. M. A Model for Magnetization Transfer in Tissues. *Magn. Reson. Med.* **1995**, *33*, 475−482.

(18) Li, J. G.; Graham, S. J.; Mark, H. R. A Flexible Magnetization Transfer Line Shape Derived from Tissue Experimental Data. *Magn. Reson. Med.* **1997**, *37*, 866−871.

(19) Edzes, H. T.; Samulski, E. T. Cross Relaxation and Spin Diffusion in the Proton NMR of Hydrated Collagen. *Nature* **1977**, *265*, 521−522.

(20) Wolff, S. D.; Balaban, R. S. Magnetization Transfer Contrast (MTC) and Tissue Water Proton Relaxation *in Vivo*. *Magn. Reson. Med.* **1989**, *10*, 135−144.

(21) Grad, J.; Mendelson, D.; Hyder, F.; Bryant, R. G. Direct Measurements of Longitudinal Relaxation and Magnetization Transfer in Heterogeneous Systems. *J. Magn. Reson.* **1990**, *86*, 416−419.

(22) Wu, X. Line shape of Magnetization Transfer via Cross Relaxation. *J. Magn. Reson.* **1991**, *94*, 186−190.

(23) Wu, J. Y.; Bryant, R. G.; Eads, T. M. Detection of Solidlike Components in Starch Using Cross-Relaxation and Fourier Transform Wide-Line ^{1}H NMR Methods. *J. Agric. Food Chem.* **1992**, *40*, 449−455.

(24) Grossman, R. I.; Gomori, J. M.; Ramer, K. N.; Lexa, F. J.; Schnall, M. D. Magnetization Transfer: Theory and Clinical Applications in Neuroradiology. *RadioGraphics* **1994**, *14*, 279−290.

(25) Wu, X.; Listinsky, J. J. Effects of Transverse Cross Relaxation on Magnetization Transfer. *J. Magn. Reson., Ser. B* **1994**, *105*, 73−76.

(26) Eads, T. M.; Axelson, D. E. Nuclear Cross Relaxation Spectroscopy and Single Point Imaging Measurements of Solids and Solidity in Foods. In *Magnetic Resonance in Food Science*; Belton, P. S., Delgadillo, I., Gil, A. M., Webb, G. A., Eds.; The Royal Society of Chemistry: Cambridge, 1995; pp 230−242.

(27) Harrison, R.; Bronskill, M. J.; Henkleman, R. M. Magnetization Transfer and T_2 Relaxation Components in Tissue. *Magn. Reson. Med.* **1995**, *33*, 490−496.

(28) Ernst, R. R.; Bodenhausen, G.; Wokaun, A. *Principles of Nuclear Magnetic Resonance in One and Two Dimensions*. Oxford University Press: U.K., 1987; pp 204−205.

(29) Caines, H. G.; Schleich, T. Incorporation of Saturation Transfer into the Formalism for Rotating-Frame Spin−Lattice NMR Relaxation in the Presence of an Off-Resonance-Irradiation Field. *J. Magn. Reson.* **1991**, *95*, 457−476.

(30) Martin, R. H. *Elementary Differential Equations with Boundary Value Problems*; McGraw-Hill Book Company: New York, 1984.

(31) Stanisz, G. J.; Kecojevic, A.; Bronskill, M. J.; Henkelman, R. M. Characterizing White Matter with Magnetization Transfer and T_2. *Magn. Reson. Med.* **1999**, *42*, 1128−1136.

(32) Miles, M. J.; Morris, V. J.; Orford, P. D.; Ring, S. G. The Roles of Amylose and Amylopectin in the Gelation and Retrogradation of Starch. *Carbohydr. Res.* **1985**, *135*, 271−281.

(33) Jane, J.; Chen, Y. Y.; Lee, L. F.; McPherson, A. E.; Wong, K. S.; Radosavljevic, M.; Kasemsuwan, T. Effects of Amylopectin Branch Chain Length and Amylose Content on the Gelatinization and Pasting Properties of Starch. *Cereal Chem.* **1999**, *76*, 629−637.

(34) Mua, J. P.; Jackson, D. S. Retrogradation and Gel Textural Attributes of Corn Starch Amylose and Amylopectin Fractions. *J. Cereal Sci.* **1998**, *27*, 157−166.

(35) Cooke, D.; Gidley, M. J. Loss of Crystalline and Molecular Order During Starch Gelatinization: Origin of the Enthalpic Transition. *Carbohydr. Res.* **1992**, *227*, 103−112.

(36) Ward, K. E. J.; Hoseney, R. C.; Seib, P. A. Retrogradation of Amylopectin from Maize and Wheat Starches. *Cereal Chem.* **1994**, *71*, 150−155.

(37) Baker, L. A.; Rayas-Duarte, P. Retrogradation of Amaranth Starch at Different Storage Temperatures and the Effects of Salt and Sugars. *Cereal Chem.* **1998**, *75*, 308−314.

(38) Paredes-Lopez, O.; Bello-Perez, L. A.; Lopez, M. G. Amylopectin: Structural, Gelatinisation and Retrogradation Studies. *Food Chem.* **1994**, *50*, 411−417.

(39) Kugiyama, M.; Donovan, J. W.; Wong, R. Y. Phase Transitions of Amylose-Lipid Complexes in Starches: A Calorimetric Study. *Starch* **1980**, *32*, 265−270.

(40) Zeleznak, K. J.; Hoseney, R. C. The Role of Water in the Retrogradation of Wheat Starch Gels and Bread Crumb. *Cereal Chem.* **1986**, *63*, 407−411.

(41) Longton, J.; LeGrys, G. A. Differential Scanning Calorimetry Studies on the Crystallinity of Aging Wheat Starch Gels. *Starch* **1981**, *33*, 410−414.

(42) Biliaderis, C. G. The Structure and Interactions of Starch with Food Constituents. *Can. J. Physiol. Pharmacol.* **1991**, *69*, 60−78.

(43) Miles, M. J.; Morris, V. J.; Ring, S. G. Some Recent Observations on the Retrogradation of Amylose. *Carbohydr. Polym.* **1984**, *4*, 73−77.

(44) Miles, M. J.; Morris, V. J.; Ring, S. G. Gelation of Amylose. *Carbohydr. Res.* **1985**, *135*, 257−269.

(45) Gidley, M. J. Molecular Mechanisms Underlying Amylose Aggregation and Gelation. *Macromolecules* **1989**, *22*, 351−358.

(46) Clark, A. H.; Ross-Murphy, S. B. Structural and Mechanical Properties of Biopolymer Gels. *Adv. Polym. Sci.* **1987**, *83*, 57−192.

(47) Clark, A. H.; Gidley, M. J.; Richardson, R. K.; Ross-Murphy, S. B. Rheological Studies of Aqueous Amylose Gels: The Effect of Chain Length and Concentration on Gel Modulus. *Macromolecules* **1989**, *22*, 346−351.

2358 *J. Agric. Food Chem.,* Vol. 51, No. 8, 2003

Lewen et al.

(48) Leloup, V. M.; Colonna, P.; Ring, S. G.; Roberts, K.; Wells, B. Microstructure of Amylose Gels. *Carbohydr. Polym.* **1992**, *18*, 189−197.

(49) Ring, S. G.; Colonna, P.; l'Anson, K. J.; Kalichevsky, M. T.; Miles, M. J.; Morris, V. J.; Orford, P. D. The Gelation and Crystallization of Amylopectin. *Carbohydr. Res.* **1987**, *162*, 277−293.

(50) Manners, D. J. Recent Developments in our Understanding of Amylopectin Structure. *Carbohydr. Polym.* **1989**, *11*, 87−112.

(51) Carriere, C. J. Evaluation of the Entanglement Molecular Weights of Maize Starches from Solution Rheological Measurements. *Cereal Chem.* **1998**, *75*, 360−364.

(52) Chinachoti, P.; White, V. A.; Lo, L.; Stengle, T. R. Application of High-Resolution Carbon-13, Oxygen-17, and Sodium-23 Nuclear Magnetic Resonance to Study the Influences of Water, Sucrose, and Sodium Chloride on Starch Gelatinization. *Cereal Chem.* **1991**, *68*, 238−244.

(53) Schmidt, S. J.; Lai, H. M. Use of NMR and MRI to Study Water Relations in Foods. In *Water Relationships in Foods*; Levine, H., Slade, L., Eds.; Plenum Press: New York, 1991; pp 405−452.

(54) Ablett, S.; Darke, A. H.; Izzard, M. J.; Lillford, P. J. Studies of the Glass Transition in Malto-oligomers. In *The Glassy State in Foods*; Blanshard, J. M. V., Lillford, P. J., Eds.; Nottingham University Press: Loughborough, Leicesetershire, 1993; pp 189−206.

(55) Cheetham, N. W. H.; Tao, L. Oxygen-17 NMR Relaxation Studies on Gelatinization Temperature and Water Mobility in Maize Starches. *Carbohydr. Polym.* **1998**, *35*, 279−286.

(56) Ohtsuka, A.; Watanabe, T.; Suzuki, T. Gel Structure and Water Diffusion Phenomena in Starch Gels Studied by Pulsed Field Gradient Stimulated Echo NMR. *Carbohydr. Polym.* **1994**, *25*, 95−100.

(57) Kou, Y.; Molitor, P.; Schmidt, S. J. Mobility and stability of model food systems using NMR, DSC, and conidia germination techniques. *J. Food Sci.* **1999**, *64* (6), 950−959.

(58) Le Botlan, D.; Rugraff, Y.; Martin, C.; Colonna, P. Quantitative Determination of Bound Water in Wheat Starch by Time Domain NMR Spectroscopy. *Carbohydr. Res.* **1998**, *308*, 29−36.

(59) Morris, K. F.; Johnson, C. S., Jr. Resolution of Discrete and Continuous Molecular Size Distributions by Means of Diffusion-Ordered 2D NMR Spectroscopy. *J. Am. Chem. Soc.* **1993**, *115*, 4291−4299.

(60) Chen, A.; Wu, D.; Johnson, C. S. J. Determination of Molecular Weight Distributions for Polymers by Diffusion-Ordered NMR. *J. Am. Chem. Soc.* **1995**, *117*, 7965−7970.

(61) Delsuc, M. A.; Malliavin, T. E. Maximum Entropy Processing of DOSY NMR Spectra. *Anal. Chem.* **1998**, *70*, 2146−2148.